SSRG International Journal of Electrical and Electronics Engineering
ISSN: 2348-8379/ https://doi.org/10.14445/23488379/IJEEE-V13I2P117

Volume 13 Issue 2, 214-230, February 2026

Original Article

Control of Standalone Hybrid Renewable Generation System with Advanced Controllers

Dharavath Chandrashekar[1], P. Satish Kumar[2]

[1,2]*Department of Electrical Engineering, Osmania University, Hyderabad.*

[1]*Corresponding Author : chandrashekar@osmania.ac.in*

Received: 20 November 2025 Revised: 24 December 2025 Accepted: 22 January 2026 Published: 17 February 2026

Abstract *- In the near future, most of the electrical power generation will rely on renewable sources with zero carbon emissions. When these renewable sources are connected to the grid in parallel, they only need synchronization controllers. This paper examines a standalone renewable system comprising a PV plant, a wind generator, and a Battery Energy System (BES) module for testing. Allthese sources are integrated to meet the local load demand. The PV plant and wind generator require MPPT modules for maximum power extraction, and the BES is connected at the common DC link. To achieve this, SMC-P&O MPPT is used for stable renewable power extraction, and inverter control is adopted with APC based AWPI controller to reduce harmonics. In further modification, the SMC MPPTs of the PV plant and wind generator are updated with a Fuzzy module for increased power extraction and faster response to variable solar irradiation. In the interfacing inverter control, the AWPI controller is replaced with a Dual Sliding Mode-Proportional Integral (DSM-PI) controller for reduced THD in the inverter voltages and currents. A comparative analysis is conducted to compare both the test systems with SMC MPPTs, AWPI, and Fuzzy SMC MPPTs,DSM-PI to validate the optimal system.*

Keywords *- PV (Photo Voltaic), MPPT (Maximum Power Point Tracking), SMC P&O (Sliding Mode Control Perturb and Observe), APC (Active Power Control), AWPI Anti-windup Proportional Integral), Fuzzy, DSM-PI Dual Sliding Mode - PI.*

1. Introduction

Renewable energy sources must be integrated more extensively into the electrical grid to reduce dependence on conventional power generation methods. These renewable sources interface with the grid via power electronic converters to enable stable, continuous power transfer. The grid may also exist as a microgrid with lower power capacity dedicated to supplying local loads [1]. For successful integration, the renewable sources must be synchronized with the grid in terms of frequency, voltage magnitude, and phase angles. Grid-connected renewable systems are comparatively more stable because they are supported by the utility grid, which acts as an infinite bus. When renewable power generation is insufficient due to increased load demand, the utility grid compensates for the deficit. Conversely, when renewable generation exceeds local demand, the surplus power is supplied back to the grid to serve other connected loads [2].

With these advantages, the grid is connected to the system. The major concern is when renewable sources are operated in a standalone condition with no grid intervention [3]. As the renewable sources are unpredictable sources with variable power generation with respect to natural source availability, it is not recommended to connect to the load directly. For the standalone renewable source system, an energy storage device can be used to support the unpredictable renewable sources. The most promising energy storage device is a Battery Energy Storage (BES) module, which has the capability to store and discharge power when needed.

The BES is placed at the DC link, where all the modules (renewable sources and loads) are connected, stabilizing the DC link voltage [4]. For the analysis of a standalone renewable source system with BES, two renewable sources, a PV module and a wind generator, are considered feeding a local load. The complete structure for the analysis is presented in Figure 1.

2. Hybrid Renewable Generation System

As shown in Figure 1, the standalone renewable energy system consists of individual DC–DC and AC–DC converters for the PV array and wind turbine, respectively. The Battery Energy Storage (BES) system is connected directly to the DC bus to facilitate power exchange [5]. The DC–DC and AC–DC converters ensure maximum power extraction from the PV and wind sources. A central inverter is connected at the DC bus to convert the combined DC power from the renewable sources and battery into AC. This AC output is supplied to residential and dump loads while maintaining regulated voltage and frequency. Both the DC–DC and AC–DC

converters are controlled using a Sliding Mode Control (SMC) based Perturb and Observe (P&O) MPPT technique, utilizing feedback signals from the source voltage and current (Vin and Iin). The central inverter is controlled using an APC-based AWPI control scheme with feedback from the three-phase load voltages and currents (VLabc and ILabc) [6]. The SMC P&O MPPT is later enhanced to an SMC-FLC MPPT to improve maximum power extraction. Additionally, the inverter controller is upgraded to a DSM-PI controller, replacing the AWPI controller, resulting in reduced reference disturbances and lower harmonic distortion at the AC output delivered to the load. This paper is structured as follows: Section 1 presents the overall standalone system outline and integrated module description. Section 2 explains the circuit configuration of each subsystem. Section 3 details the controller design with multi-signal feedback. Section 4 provides simulation results and performance analysis for different controller configurations. Section 5 concludes the work and identifies the optimal controller for the proposed standalone renewable system.

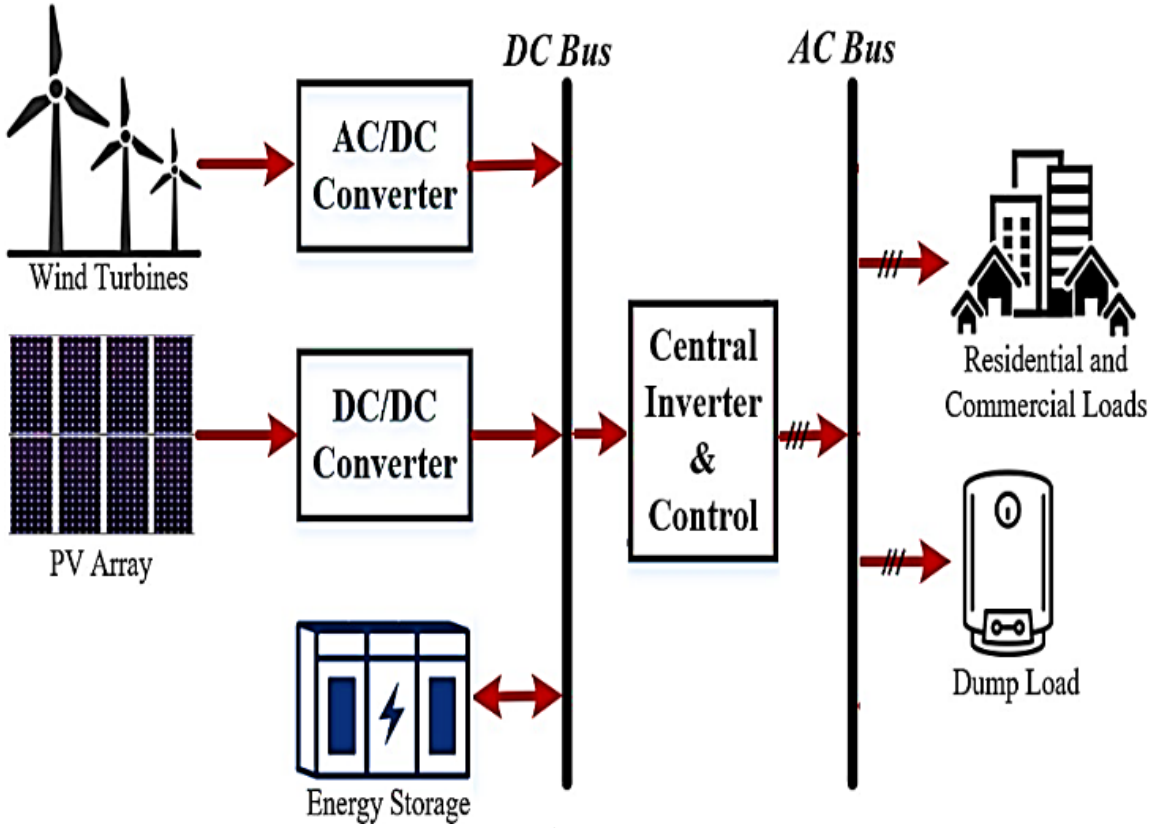

Fig. 1 Overall schematic of a standalone renewable system

3. Proposed Advanced Controller for a Hybrid Renewable Generation System

As mentioned previously in section 1, the proposed standalone renewable system comprises two renewable sources: a PV module and a wind generator. Along with these two renewable sources, an energy storage device (battery pack) is connected at the DC link for DC voltage stability [7]. The PV module comprises several PV panels interconnected in combinations of series and parallel for an increment of voltage and current as per the requirement. As the PV panels generate power as DC voltage, they need a simple DC/DC converter for voltage boost and stabilization. However, in the wind generator, a PMBLDCG machine is used for the generation ofpower [8]. The PMBLDCG receives rotational torque from wind turbines propelled by wind hitting the blades. As the considered system is a miniature rating, the wind generator uses micro turbines for the generation of electricity. The complete structure, including the renewable sources and BES module with the connected power circuits compensating a load, is presented in Figure 2. As shown in Figure 1, the PV module and the wind generator are each integrated with a DC–DC boost converter, using a single IGBT switch. Since the PMBLDC generator produces an uncommutated trapezoidal AC output, a Diode Bridge Rectifier (DBR) is connected at the generator terminals [9]. The DBR converts the trapezoidal AC voltage into DC, which then serves as the input to the boost converter. The battery pack is connected to the DC link, which is directly interfaced with the DC–AC inverter to support power balancing and storage functions [10]. An LC filter is placed between the inverter and the load to reduce harmonic components, designed according to the inverter switching frequency and

maximum load rating. The system employs three independent controllers: one for the PV module, one for the wind generator, and one for the inverter. The PV and wind controllers share the same control structure, with differences only in their input sensing variables. The inverter controller operates based on feedback signals measured from the load side. The detailed structure of these controllers, along with the corresponding design equations, is discussed in the following section.

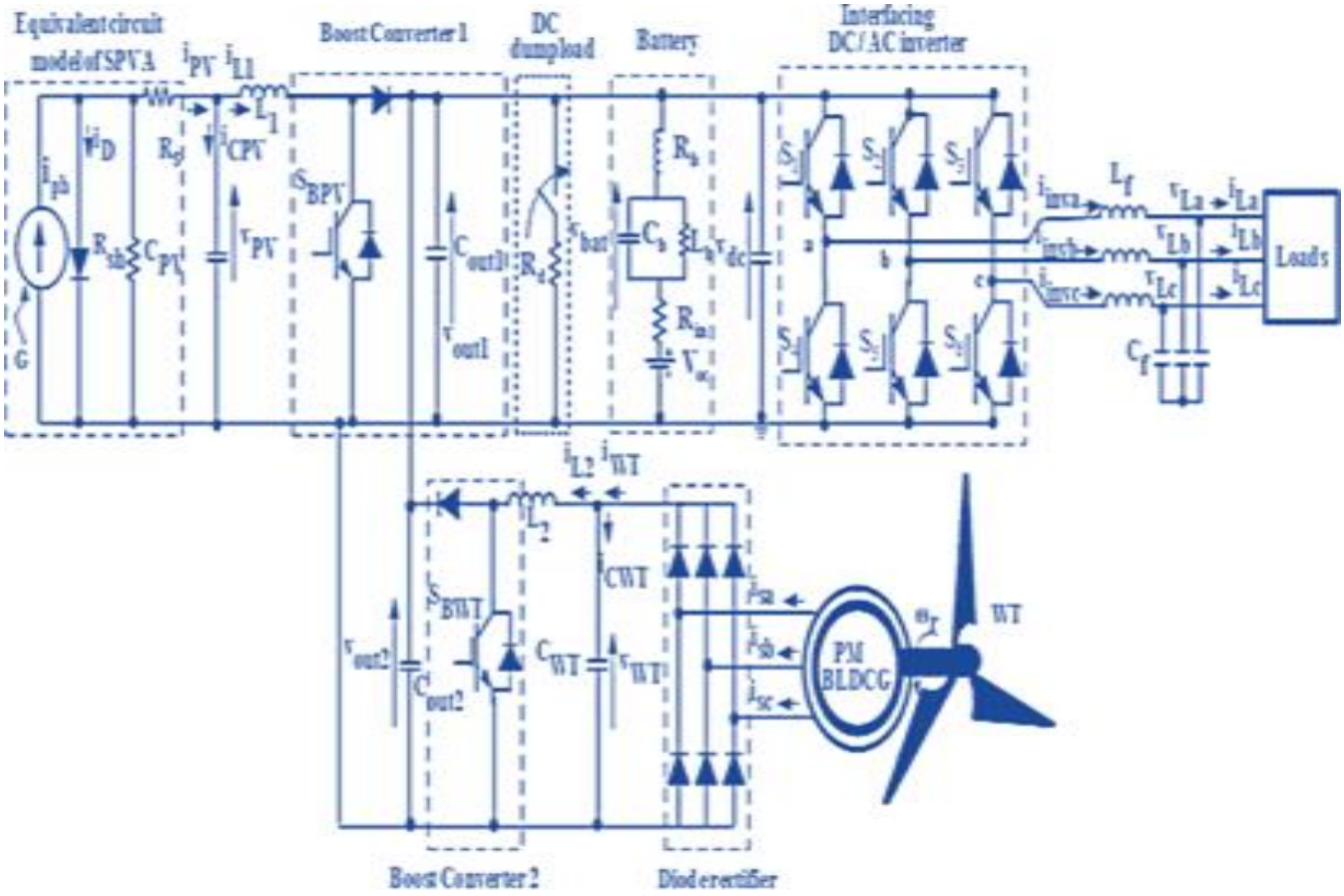

Fig. 2 Circuit structure of a standalone renewable system

3.1 Sliding Mode Control Perturb and Observe MPPT (SMC P&O MPPT)

In most of the conventional MPPT techniques, the P&O method is commonly used for maximum power extraction from the renewable sources. Any MPPT method needs input voltage (V_{in}) and input current (I_{in}) as reference signals for the generation of either reference voltage (V_{ref}) or duty ratio (D) [11]. With faster response to input signals, the MPPT method is considered better. In this paper, a 'modified P&O MPPT' technique with SMC is integrated for controlling the IGBT switch of the DC/DC boost converter. Figure 3 is the control structure of the SMC P&O MPPT module used for the generation of the duty ratio.

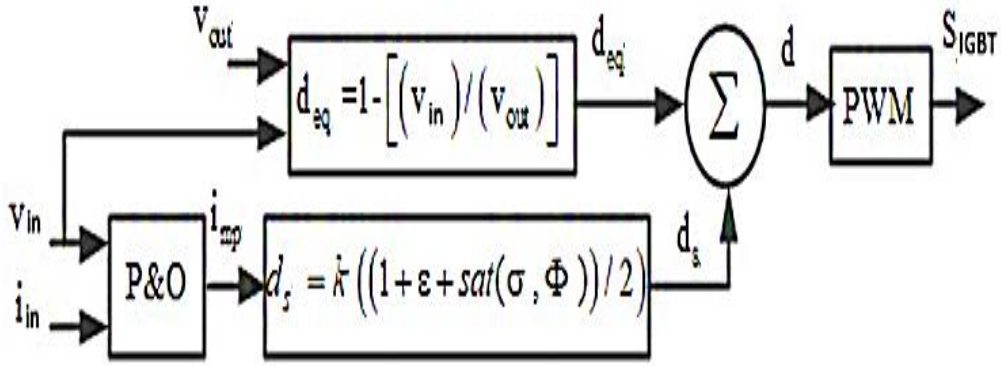

Fig. 3 SMC P&O MPPT structure

As per the given structure, the final duty ratio (d) is the addition of two duty ratio factors, d_{eq} and d_s, which are generated by multiple variables [6]. The final duty ratio (d) is given as:

$$d = d_{eq} + d_s \tag{1}$$

$$d_{eq} = 1 - \left[\frac{v_{in}}{v_{out}}\right] \tag{2}$$

$$d_s = \frac{k}{2}(1 + \varepsilon + sat\ (\sigma, \varphi)) \tag{3}$$

As per expressions (2) and (3) v_{in} and v_{out} These are the input and output voltages of the DC/DC boost converter. These variables determine the duty factor d_{eq}, whereas the d_s duty factor is determined by variables 'k' and 'ε', which are the controller gain and error coefficient, respectively [6]. The $sat\ (\sigma, \varphi)$ is determined as:

$$sat\ (\sigma, \varphi) = \begin{cases} 1\ if\ \sigma > \varphi \\ \frac{\sigma}{\varphi}\ if\ |\sigma| \leq \varphi \\ -1\ if\ \sigma < \varphi \end{cases} \tag{4}$$

Here, φ is the sliding layer value considered between -0.5 and 0.5. And the σ is calculated as:

$$\sigma = v_{in} + i_{mp}\left(\frac{dv_{in}}{di_{mp}}\right) \tag{5}$$

Here, i_{mp} is the estimated current at maximum power determined by the classic P&O MPPT technique, dv_{in} and di_{mp} are the changes in v_{in} and i_{mp}. The i_{mp} the value is calculated by the following comparative expression generated by the P&O MPPT technique.

$$i_{mp} = i_{mp}(t-1) + \Delta D \begin{Bmatrix} If\ P(t) > P(t-1)\ and\ V(t) > V(t-1) \\ If\ P(t) < P(t-1) amd\ V(t) < V(t-1) \end{Bmatrix} \tag{6}$$

$$i_{mp} = i_{mp}(t-1) - \Delta D \begin{Bmatrix} If\ P(t) < P(t-1)\ and\ V(t) > V(t-1) \\ If\ P(t) > P(t-1) amd\ V(t) < V(t-1) \end{Bmatrix} \tag{7}$$

Here, $i_{mp}(t-1)$ is the previous value of i_{mp}, ΔD is the updated variable to the i_{mp} increase or decrease as per conditions. V(t) and P(t) represent the present values of the input voltage and power to the boost converter, respectively, while V(t−1) and P(t−1) denote their previous values [12]. The duty ratio (d) obtained from these expressions is compared with a high-frequency triangular carrier signal to generate the PWM pulse for driving the IGBT switch of the boost converter. Sliding control of the duty ratio ensures maximum power extraction, and the extracted power is delivered to the DC link. Each renewable source converter employs its own SMC P&O MPPT technique integrated within the respective module.

3.2. Modified Fuzzy MPPT Technique

For improving the performance of the MPPT module, the conventional MPPT method is replaced with the Fuzzy MPPT module. The Fuzzy MPPT module is considered to be a fast, responsive algorithm for the changes in the input voltage and current. The novel fuzzy MPPT methods need two input variables $\frac{dP}{dI}$ and $d\left(\frac{dP}{dI}\right)$ which are denoted as the ratio of change in input power (dP) by change in input current (dI) and change in the calculated ratio, respectively [15]. The output variable of the fuzzy MPPT is also the duty ratio d of the boost converter switch. The modeling of the fuzzy MPPT is presented in Figure 4, modeled using Simulink software.

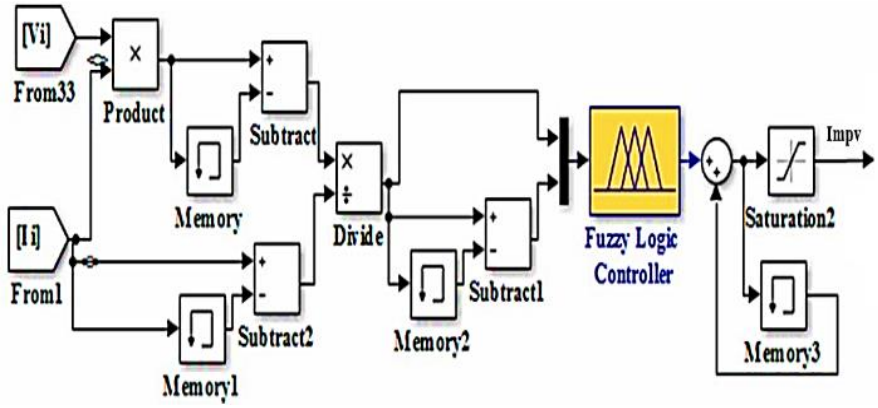

Fig. 4 Fuzzy MPPT module

In Figure 5, the memory block creates a unit delay, which generates the previous value of the input signal. Each variable is included with five Membership Functions (MFs) using a 'triangular shape' type.

The MFs are arranged in specific ranges as per the input signal value range estimation. Figure 5 shows the MFs of the input and output variables of the Fuzzy MPPT.

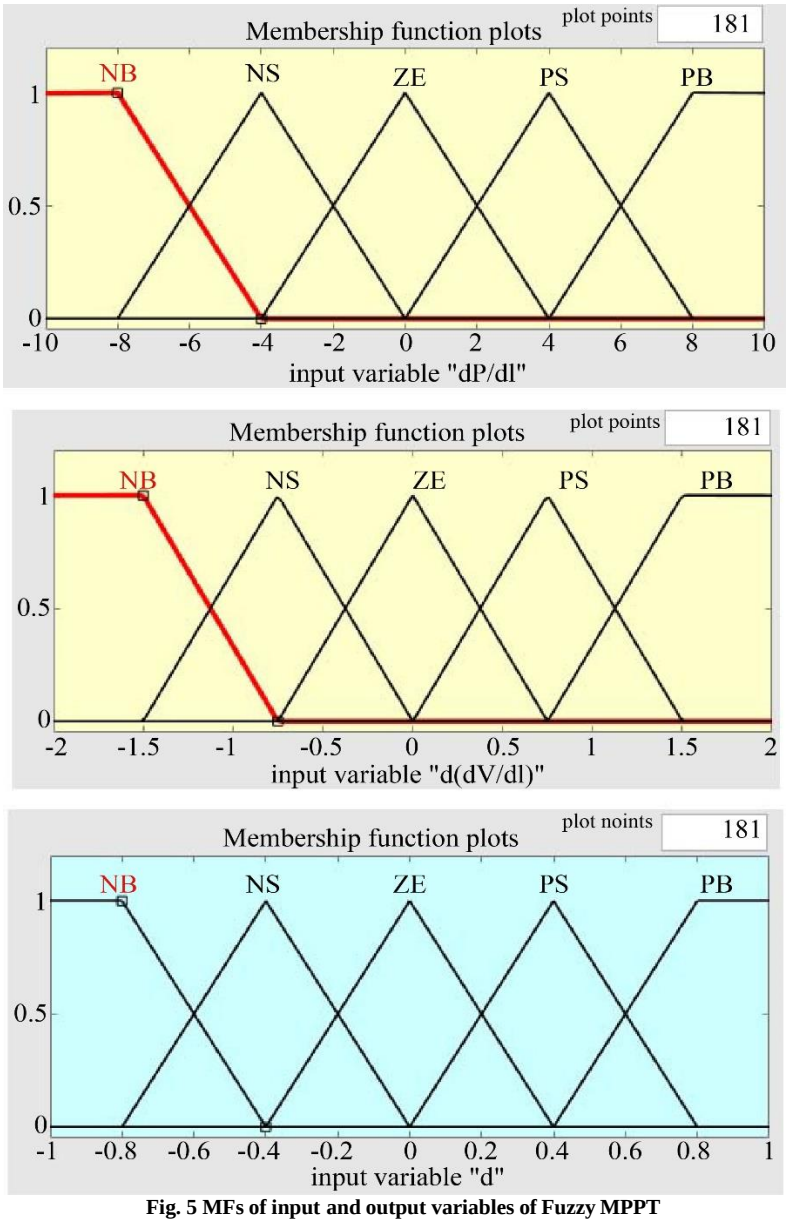

Fig. 5 MFs of input and output variables of Fuzzy MPPT

The MFs of the variables are named as PB (Positive Big), PS (Positive Small), ZE (Zero), NS(Negative Small), and NB (Negative Big) with respect to the placement range. The $\frac{dP}{dI}$ is set with -10 to 10, and $d\left(\frac{dP}{dI}\right)$ is set with -2 to 2, and d is set with -1 to 1 range [16]. As per the MFs set in the tool, the 25th rule is updated accordingly using an IF-AND-THEN relation [15]. Table 1 is the rule base for the proposed Fuzzy MPPT module of the journal. As per the rule base, the output duty ratio 'd' is generated, which is varied as per the change insolar irradiation (Ir).

Table 1. 25 rule-based

25 rule-based		***dP - dI***				
		NB	**NS**	**ZE**	**PS**	**PB**
$d\left(\frac{dP}{dI}\right)$	NB	PS	PS	ZE	NS	NS
	NS	PB	PS	ZE	NS	NB
	ZE	NB	NS	ZE	PS	PB
	PS	NB	NS	ZE	PS	PB
	PB	NS	NS	ZE	PS	PS

4. Active Power Control based Anti-Windup Proportional Integral (APC-based AWPI Controller)

The APC-based AWPI controller is employed to regulate the interfacing inverter between the DC link and the load. It uses feedback signals from the load voltage and current to maintain a stable output voltage magnitude and frequency [13]. Figure 6 illustrates the complete control architecture of the proposed APC-based AWPI controller, implemented with a sinusoidal PWM scheme.

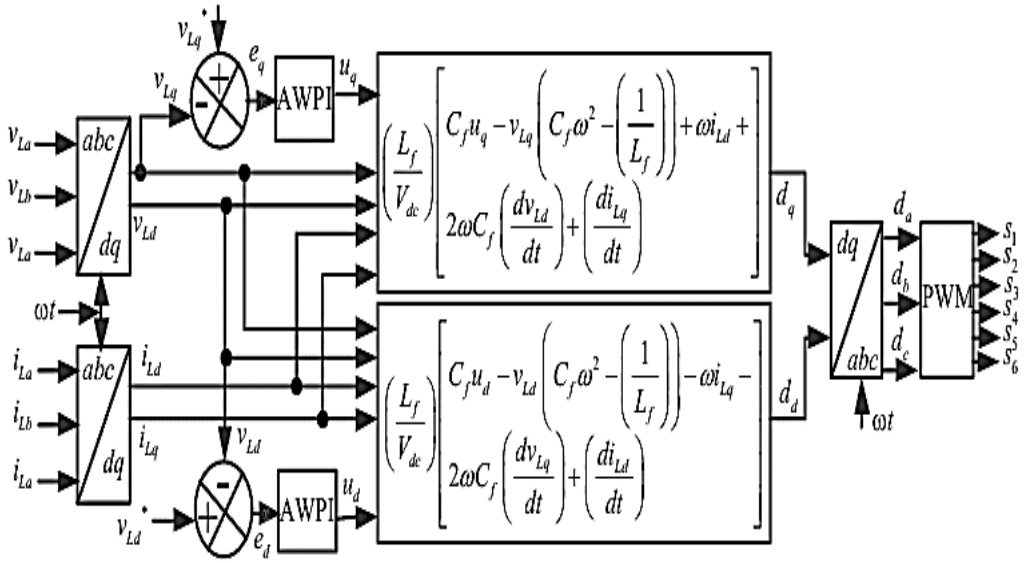

Fig. 6 APC base AWPI controller of the interfacing inverter module

The reference signals to the Sinusoidal PWM generator are generated by dq components (d_d and d_q). The controller depends on the dq component of load voltages and currents for the generation of reference signals. The dq components for VLabc and ILabc are generated using Park's transformation as expressed below.

$$\begin{bmatrix} f_d \\ f_q \end{bmatrix} = \begin{bmatrix} Sin\,\theta & -Cos\,\theta & 0 \\ Cos\,\theta & Sin\,\theta & 0 \end{bmatrix} \begin{bmatrix} f_a \\ f_b \\ f_c \end{bmatrix} \quad (8)$$

Here, 'f' can be any signal, either VL or IL, and 'θ' is the phase angle of phase A determined by the PLL (Phase Lock Loop) block. The PLL is fixed with a 50Hz fundamental frequency for the operation of the inverter at the specified frequency. From the VL and IL dq components achieved from expression (6), the reference signals d_d and d_q are generated as:

$$d_d = \frac{L_f}{V_{dc}}\left[C_f u_d - v_{Ld}\left(C_f w^2 - \left(\frac{1}{L_f}\right)\right) - \omega i_{Lq} - 2\omega C_f\left(\frac{dv_{Lq}}{dt}\right) + \left(\frac{di_{Ld}}{dt}\right)\right] \quad (9)$$

$$d_q = \frac{L_f}{V_{dc}}\left[C_f u_q - v_{Lq}\left(C_f w^2 - \left(\frac{1}{L_f}\right)\right) + \omega i_{Ld} + 2\omega C_f\left(\frac{dv_{Ld}}{dt}\right) + \left(\frac{di_{Lq}}{dt}\right)\right] \quad (10)$$

Here, V_{dc} is the measured DC link voltage, L_f and C_f are the filter inductance and capacitance values, ω is the fixed angular frequency (2.π.50), $\frac{dv_{Ld}}{dt}$ $\frac{dv_{Lq}}{dt}$ and $\frac{di_{Ld}}{dt}$ $\frac{di_{Lq}}{dt}$ are the changes in dq VL and IL values. The u_d and u_q components are generated using error dq components fed to the AWPI controller [6]. The u_d is generated by the error component comparing $v_{Ld}^*$and v_{Ld}. Similarly, u_q is the generated error component compared to $v_{Lq}^*$and v_{Lq}.

$$e_d = v_{Ld}^* - v_{Ld} \quad (11)$$

$$e_q = v_{Lq}^* - v_{Lq} \quad (12)$$

The internal modelling of the AWPI controller with input and output signals is presented in Figure 7.

Similar to a conventional PI controller, the AWPI controller has fixed proportional gain 'k'. The integral gain is varied as per the error signal (e) of the dq voltage components [14]. The u_d and u_q signals are given as:

$$u_d = e_d\left(\frac{k\tau_c(\tau_i s+1)}{\tau_i(\tau_c s+1)}\right) + u_{d\,max}\left(\frac{1}{(\tau_c s+1)}\right) \quad (13)$$

$$u_q = e_q\left(\frac{k\tau_c(\tau_i s+1)}{\tau_i(\tau_c s+1)}\right) + u_{q\,max}\left(\frac{1}{(\tau_c s+1)}\right) \quad (14)$$

Where, τ_i and τ_c are the integral gain coefficients, which are tuned as per the response of the system.

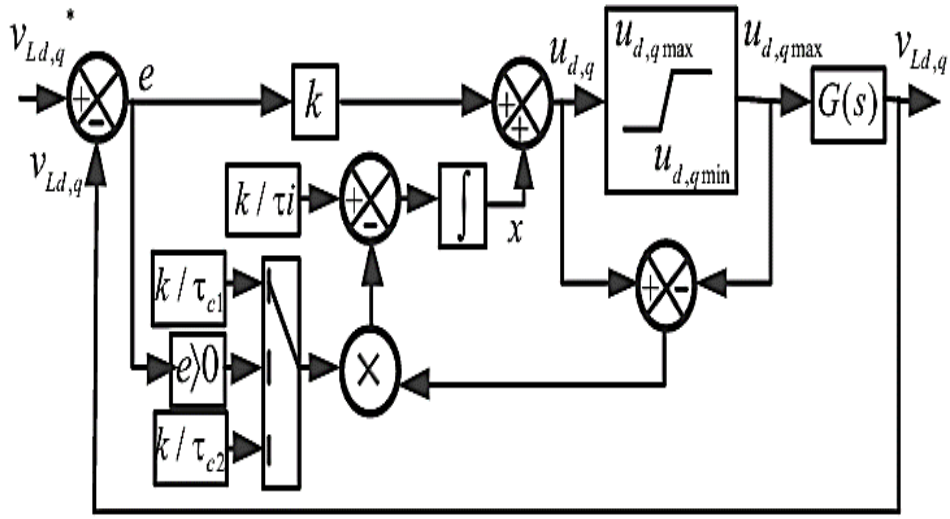

Fig. 7 AWPI controller internal structure

4.1 Dual Sliding Mode Proportional Integral (DSM-PI DESIGN)

The DSM-PI controller is an advanced control approach featuring dual variable gains to achieve faster and more stable dynamic response. In the proposed inverter control scheme it replaces the conventional AWPI controller [17]. The controller regulates the dq-axis load-voltage-error components while minimizing signal noise. The modified control structure incorporating the DSM-PI controller in place of the AWPI controller is shown in Figure 8.

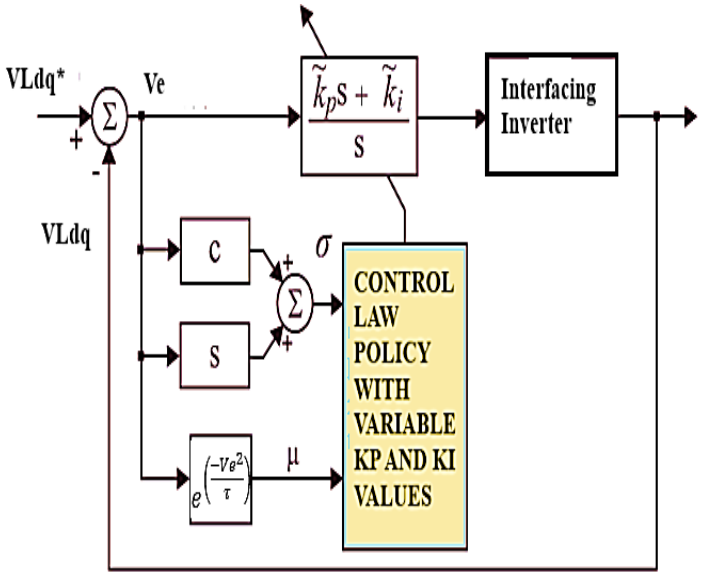

Fig. 8 DSM-PI controller internal design

According to the given control structure, the k_p and k_i gain values of the conventional PI controller are adjusted dynamically based on the selected control law. The control law policy needs two variables $'\sigma' \; and \; '\mu'$ (gain coefficients) to determine the k_p and k_i gain values [18]. These two variables $'\sigma' \; and \; '\mu'$ are dependent values of the error signal generated by a comparison of the dq components of the load voltages. They are expressed as per the equations given below:

$$\sigma = V_e.c + V_e s \tag{15}$$

$$\mu = e^{\left(\frac{-Ve^2}{\tau}\right)} \tag{16}$$

With the calculated variables $'\sigma' \; and \; '\mu'$, the control law policy equations are expressed as:

$$k_p = [(1 + sign(\sigma)k_p^+ - (1 - sign(\sigma))k_p^-] + k_p^{avg} \tag{17}$$

$$k_i = [(1 + sign(\sigma)k_i^+ - (1 - sign(\sigma))k_i^-] + k_i^{avg} \tag{18}$$

Here, k_p^+, k_p^- and k_p^{avg} are the positive, negative, and average gain values of the proportional gain. k_i^+, k_i^- and k_i^{avg} are the positive, negative, and average gain values of the integral gain [18].

These updated gain values are applied to the PI controller within the DSM-PI module to regulate the inverter voltage and current. All circuit configurations and control schemes are modeled and simulated under various operating conditions, and their performance is validated in the following section.

5. Results

The complete modeling of the standalone renewable source system with the BES module compensating the local load is done in the Simulink environment. The blocks from 'Specialized Power Systems' in the library browser are considered for the modeling of the system. Differentblocks from 'Electrical sources', 'Passive elements', 'Power electronics', and 'Commonly Used Blocks' subsets are imported for the modeling. The parameters of the modules are updated as per the configuration values in Table 2, and the simulation is run for different conditions. As per the given parameters in Table 2, the standalone renewable system is updated.

The values of each passive element of the circuit topologies and the controller gain values are given basedon stability tuning of the system. After updating the parameters, a simulation is carried out using Discrete analysis by the 'Tustin' solver type set in the 'powergui' block for the generation of graphical plots. All the voltages, powers, and currents of each module are plotted with simulation time as reference and are given below.

The simulation is run for 1sec with constant solar irradiation and wind speed set at 1000W/m² and 12m/s throughout the simulation. Figure 9 shows characteristics of the PV array with 420V V_{pv} and 19A I_{pv}. The total power generated by the PV array is 8kW, which is either shared with the load or stored in a battery pack as per the power demand. For the 12m/sec wind speed, the characteristics of PMBLDCG are presented in Figure 10.

Table 2. Configuration values of modules

Name of the module	Parameters
PV module	Manufacturer: SunPower SPR-305E-WHT-D V_{mp} = 54.7V, I_{mp} = 5.58A, V_{oc} = 64.2V, I_{sc} = 5.96A, N_s = 7, N_p = 5, P_{pv} = 10.6kW Boost converter: C_{in} =100µF, L_b = 1mH, R_{igbt} = 0.01Ω, $V_{f\,diode}$ = 0.8V
Wind module	PMBLDCG: 560Vdc, 35.17Nm, 3000rpm R_s = 0.06Ω, L_s = 0.525mH, Φ = 0.1119V.s, J = 0.0022kg.m², F = 0.000425N.m.s, p =4 Boost converter: C_{in} =1000µF, L_b = 1mH, R_{igbt} = 0.01Ω, $V_{f\,diode}$ = 0.8V
Battery	Lithium Ion 70kWhr: V_{nom} = 760V, Capacity =100Ah,
Inverter	R_{igbt} = 1mΩ, L_f = 1mH, C_f = 100µF
SMC MPPT	$\Delta D = \pm 1$, MPPT gain = 5, k = 0.017, e = 0.05, φ = -0.5, f_s = 5kHz
Active power control	V_{Ld}* = 240Vrms ph, V_{Lq}* = 0, F_n = 50Hz, k = 10, r_i = 0.01, r_{c1} = 0.1, r_{c2} = 10, f_s = 5kHz

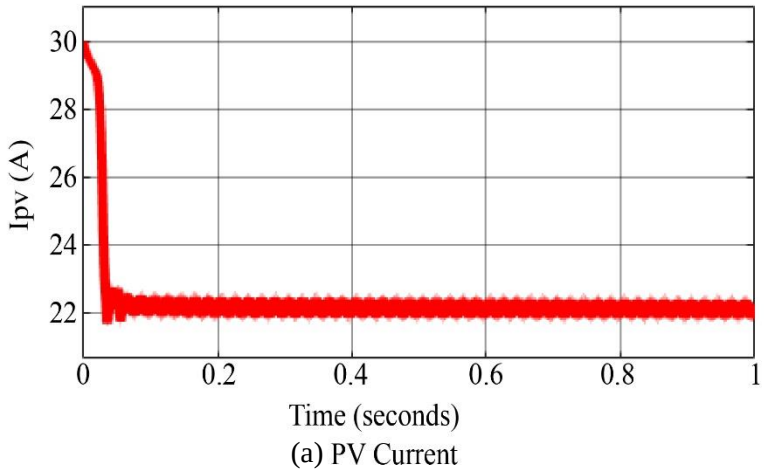

(a) PV Current

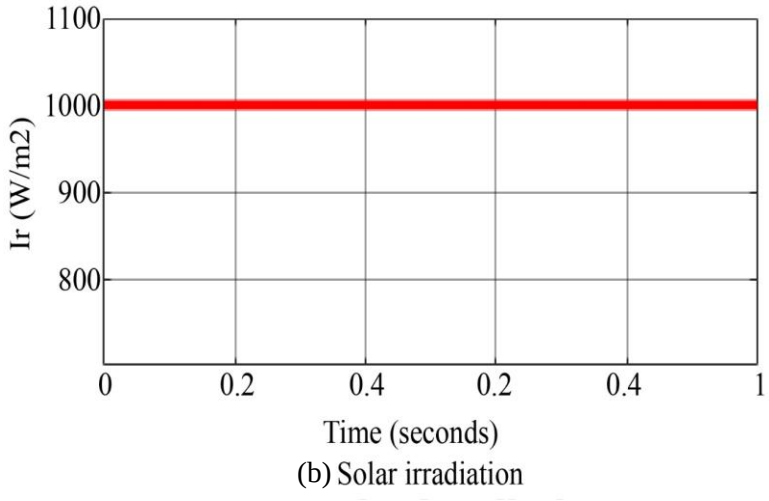

Fig. 9 PV array characteristics

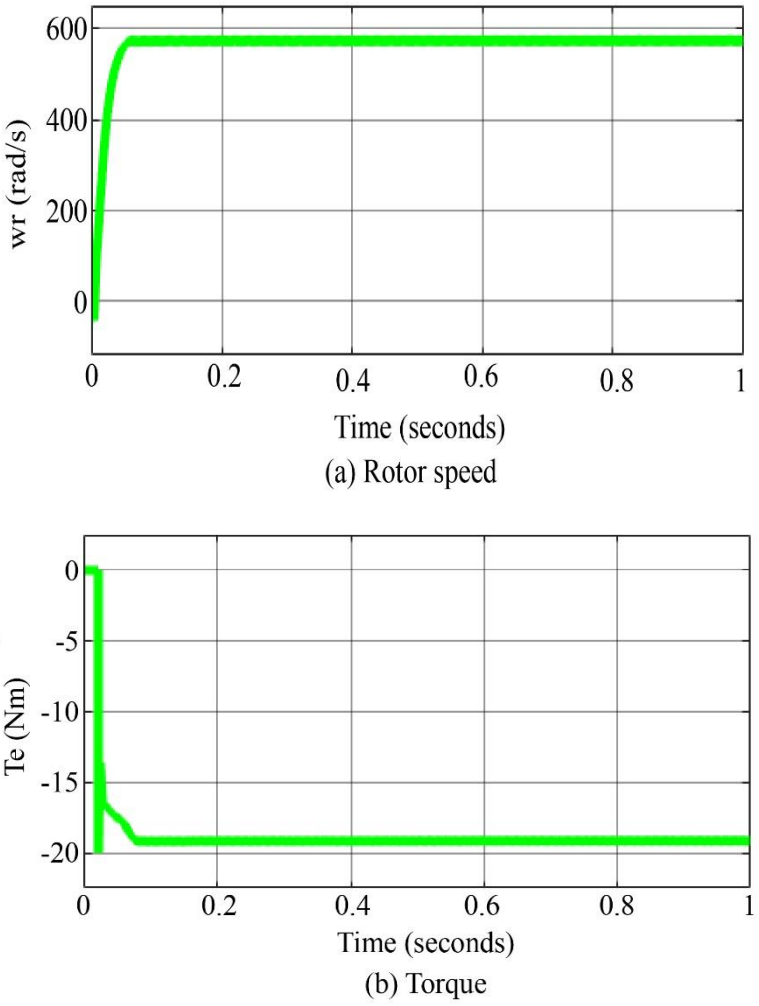

Fig. 10 PMBLDCG characteristics

As per the PMBLDCG characteristics, the speed of the machine is recorded at 600 rad/sec, and the electromagnetic torque is -16Nm. The negative torque of the measurement is denoted as a generator in the Simulink software. The total power generated by the wind generator is 9.5kW.

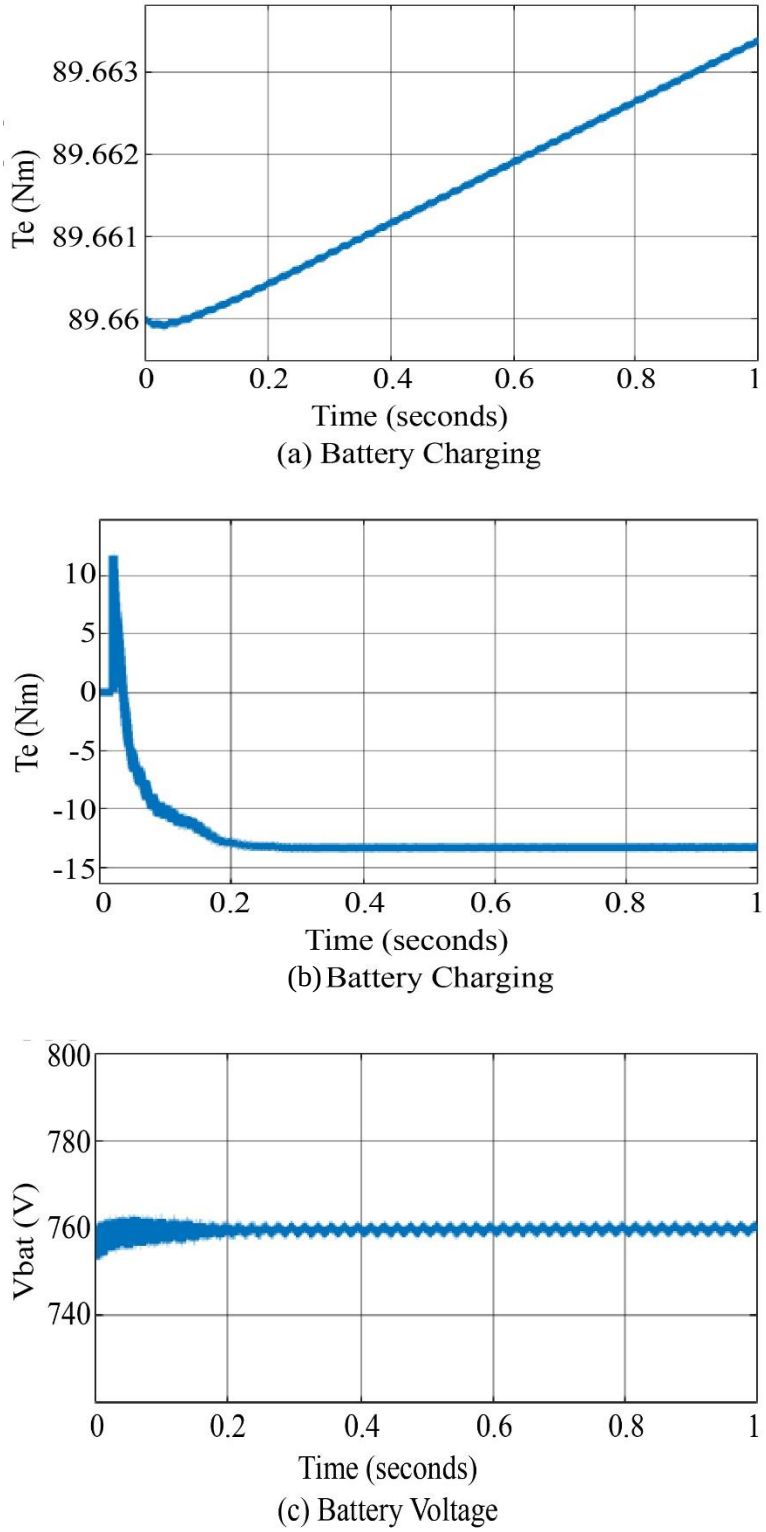

Fig. 11 Battery pack characteristics

Since the battery pack is connected at the DC link, it absorbs the excess power remaining after the load demand is met. The characteristics of the battery pack are shown in Figure 11. An increase in the SOC along with a negative current indicates that the battery is being charged from the available renewable power. The battery voltage remains around 750 V, which corresponds to its nominal voltage level at an initial SOC of 90 percent.

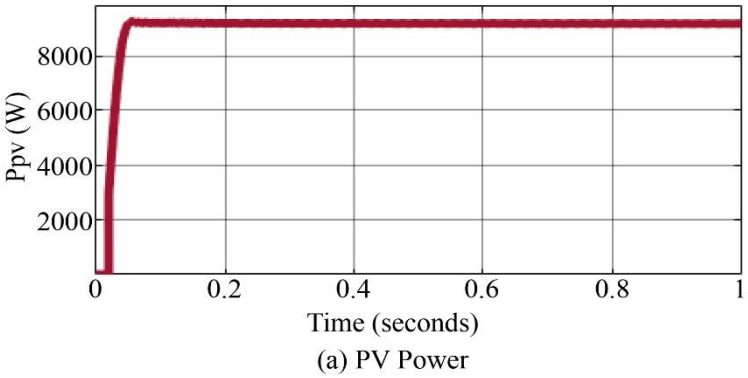

(a) PV Power

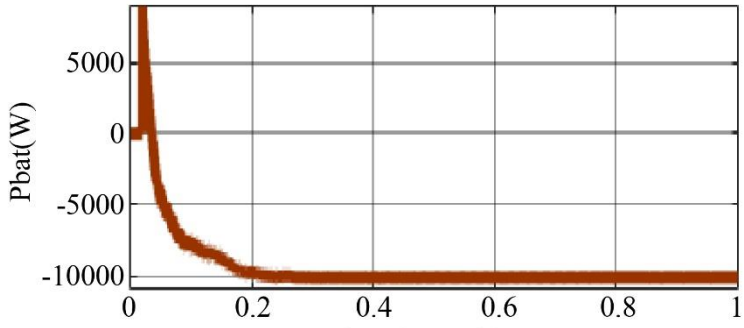

(b) Battery Power

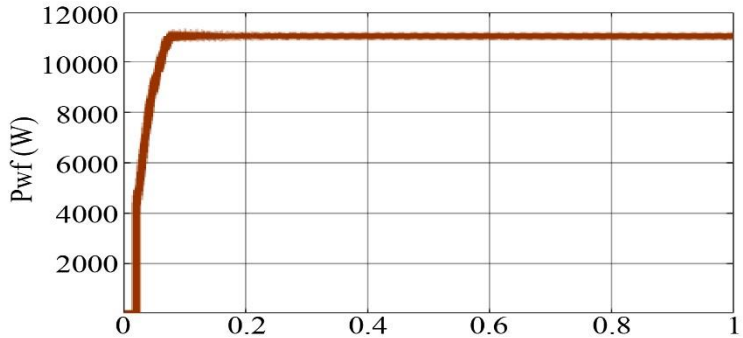

(c) Battery Power

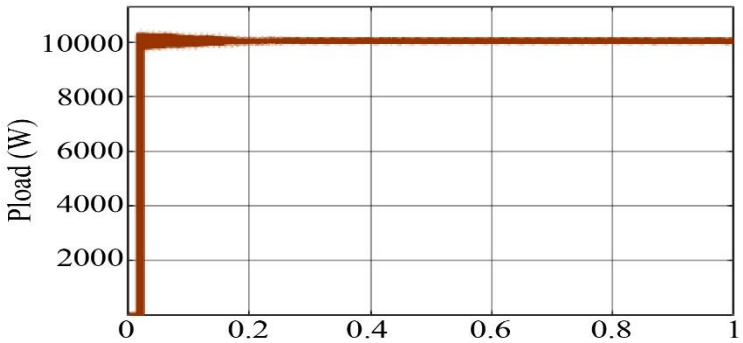

(d) Load Power

Fig. 12 Active powers of all modules

Figure 12 shows the active powers of the PV source, battery pack, wind generator, and load demand after the consumption of 10kW by the load. The remaining renewable power of 7.5kWis stored in the battery pack, represented in a negative direction.

At the output of the inverter after the LC filter, phase voltages and currents are measuredand are presented in Figure 13. From the three-phase voltages and currents, the active and reactive powers of the power delivered by the inverter are presented in Figure 14.

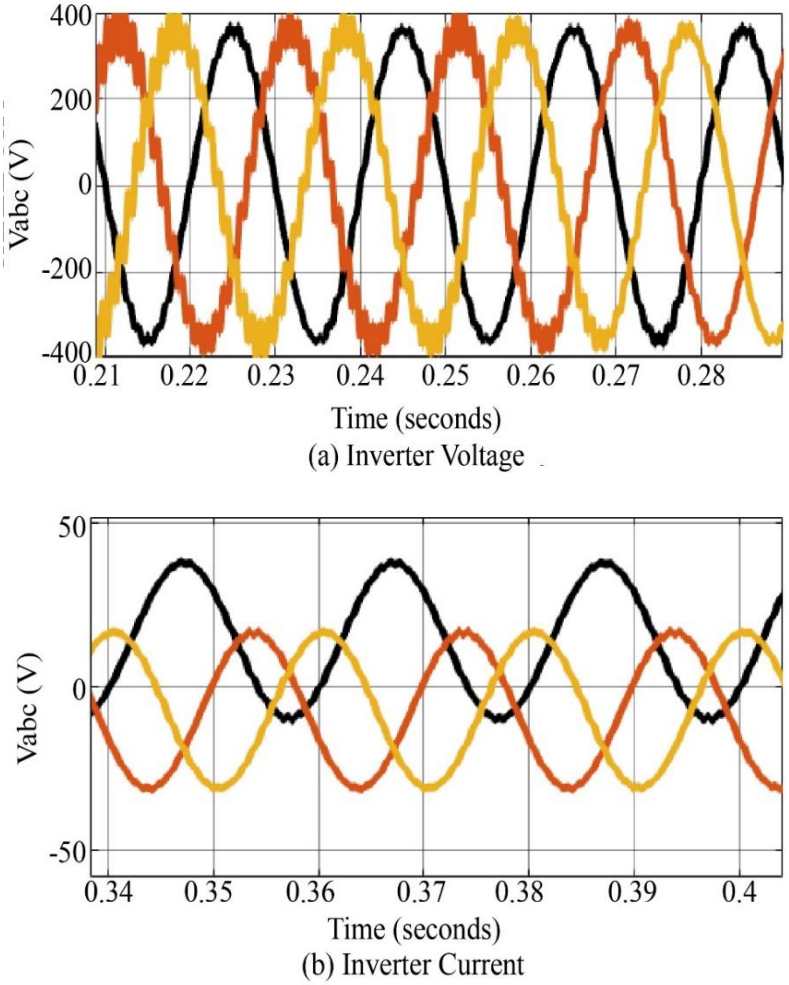

Fig. 13 Interfacing inverter voltages and currents

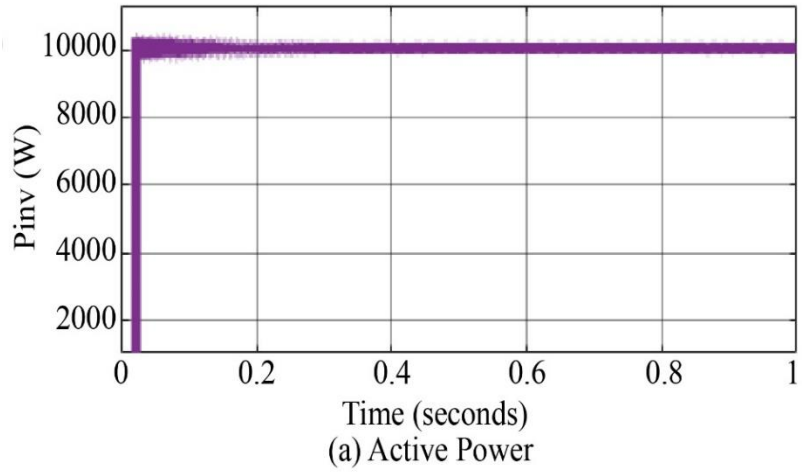

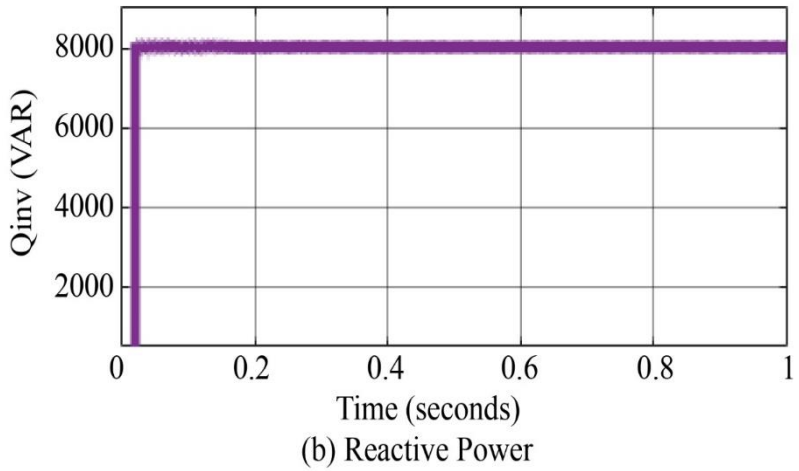

Fig. 14 Interfacing inverter active (P) and reactive (Q) powers

The system is now updated to use Fuzzy MPPT, replacing P&O MPPT, in the SMC module for optimal control of the boost converters. The fuzzy MPPT is updated in both the PV module and the wind generator boost controllers, and a simulation is run for the same rating and time. Figure 15 is the rule base generated by the fuzzy tool for the generation of variable updates to Imp. After the Fuzzy MPPT updates the active powers from the PV source and wind generator, they are recorded and compared with the conventional MPPT technique.

The PV power extraction is increased from 8kW to 9.2kW, and the wind generator power is increased from 9.5kW to 10.2kW as plotted in Figure 15. There is a significant increase in PV module and wind generator powers, increasing the total extracted power by 1.9kW, improving the performance of the boost converters. With the update of the DSM-PI controller in inverter control, the THDs (Total Harmonic Distortions) of the inverter voltage and current are calculated using the FFT analysis tool and are presented in Figures 17 and 18.

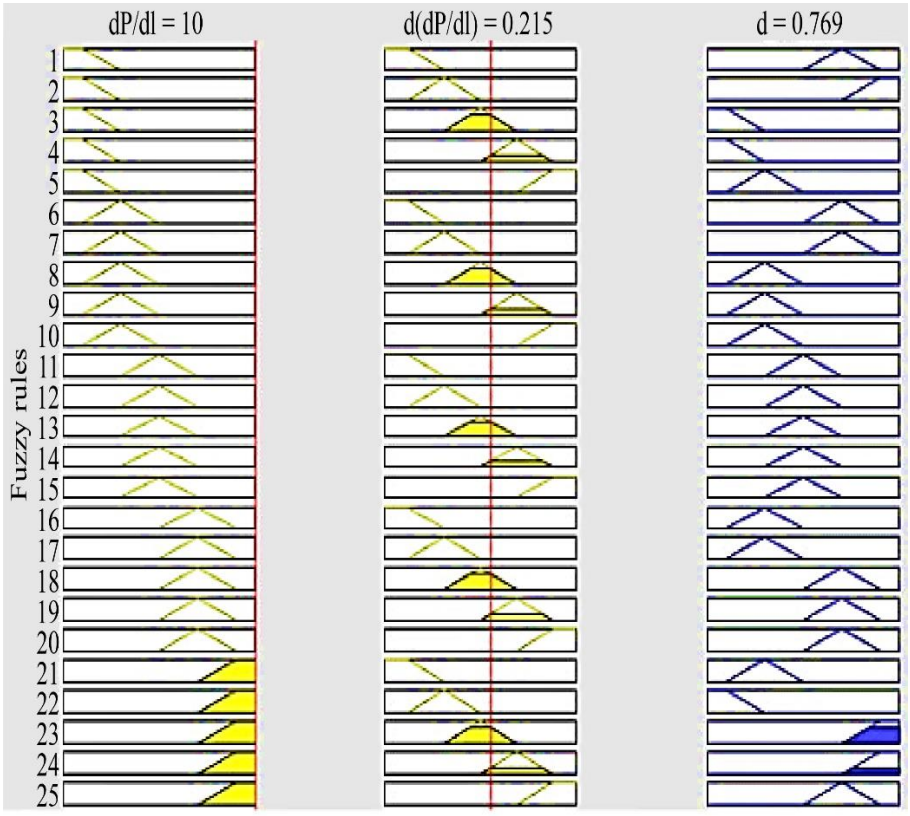

Fig. 15 Rule viewer of Fuzzy MPPT

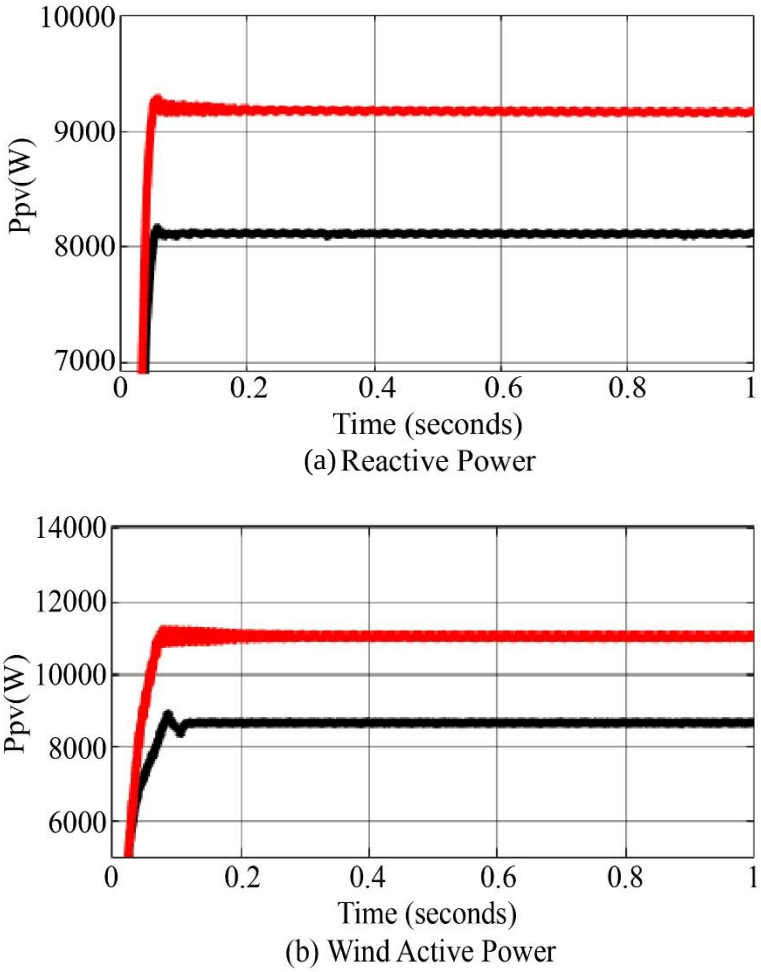

Fig. 16 PV module and wind generator active powers comparison

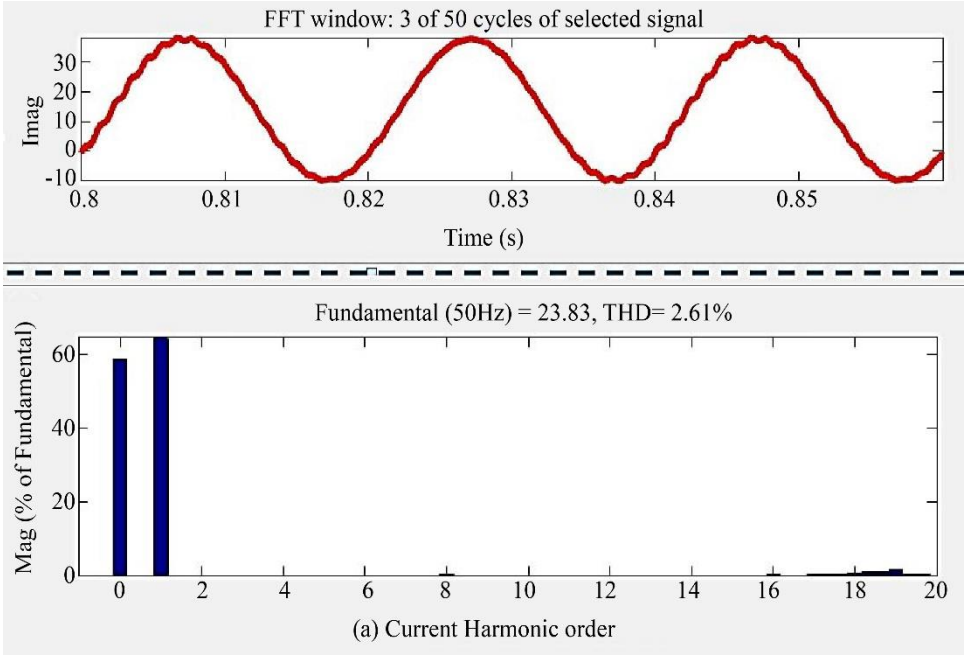

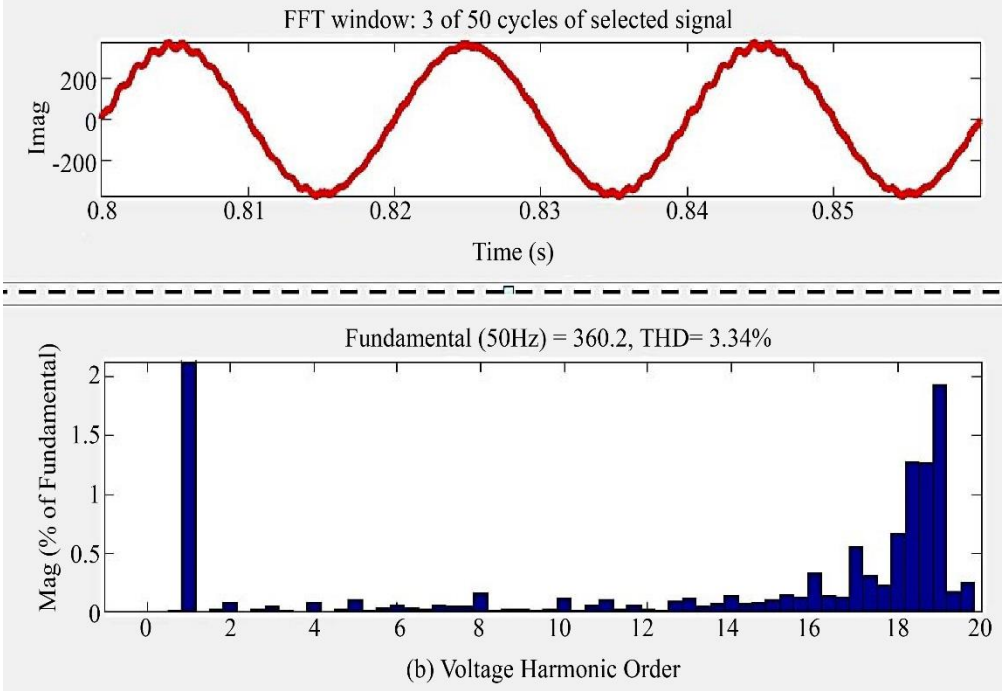

Fig. 17 FFT analysis of (a) Inverter current, and (b) Inverter voltage with AWPI controller.

Table 3. Comparisons

Name of theparameters	SMC P&O MPPT andAWPI	SMC Fuzzy MPPT andDSM-PI
P_{pv}	8kW	9.2kW
P_{wg}	9.5kW	10.2k
Vinv THD	3.34%	2.53%
Iinv THD	2.61%	1.98%

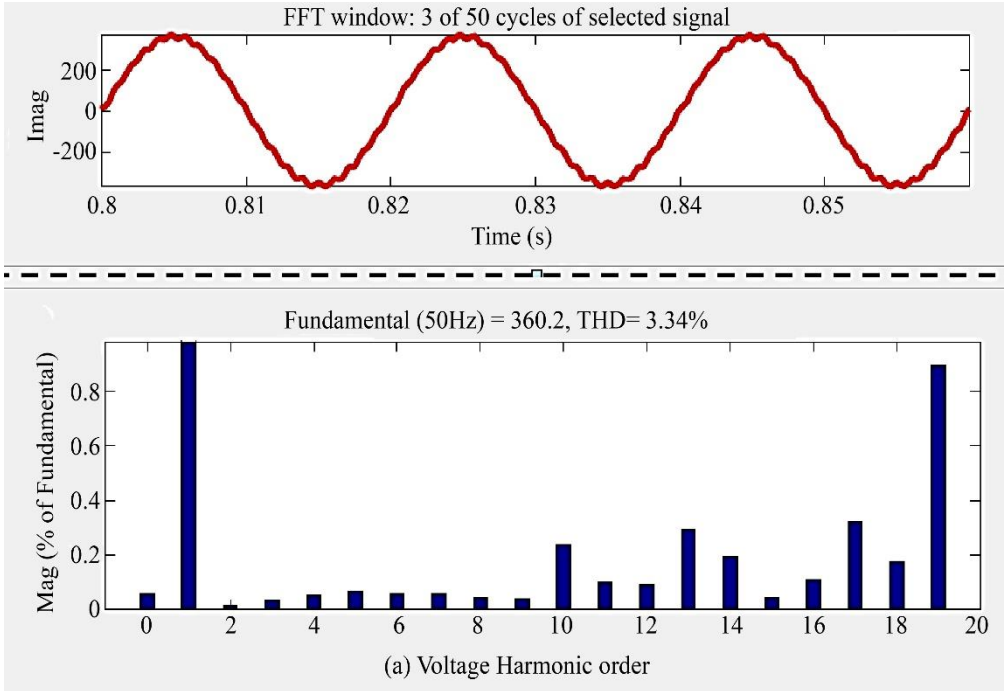

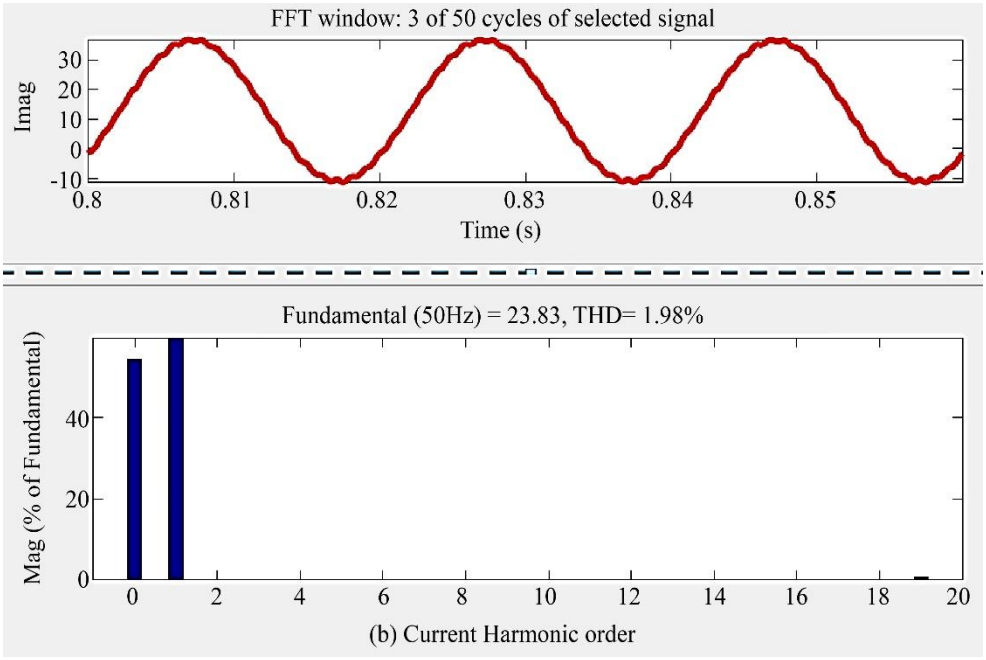

Fig. 18 FFT analysis of (a) Inverter voltage, and (b) Inverter current with DSM-PI controller.

As per the calculated THDs of the voltage and current with SMC P&O MPPT and SMC FuzzyMPPT, the values are lower, as observed in Figures 17 and 18. A comparative table with values of the recorded graphs is presented in Table 3.

6. Conclusion

A standalone renewable system with BES backup module is modelled with advanced MPPT techniques and APC-based AWPI inverter control. The PV module and the wind generator are included with individual power extraction converters operated by SMC P&O MPPT techniques. The MPPT module ensures stable voltage generation with maximum powerextraction from the renewable sources. The extracted renewable power is either stored in a battery or consumed by the local load as per the requirement. Further improvement of the system, the conventional P&O MPPT is replaced by Fuzzy MPPT for optimal power extraction. By replacing the MPPTs of both the PV module and the wind generation, the maximum power extraction is increased by 1.2kW and 0.7kW, respectively. The total power increment is noted to be 1.9kW when the same rating system is operated with the SMC Fuzzy MPPT technique. Along with the power increment due to better dq signals stability achieved by the DSM-PI controller, theTHD of the interfacing inverter three-phase voltages and currents is also improved. The total harmonics distortion of the voltage and current is reduced from 3.34% to 2.53% from 2.61% to1.98% for AWPI and DSM-PI, respectively. This THD can further be reduced by integrating advanced controllers and techniques in the active power control of the inverter.

References

[1] T. Adefarati et al., “Design and Feasibility Analysis of Grid-Connected Hybrid Renewable Energy System: Perspective of Commercial Buildings,” *Energy Systems*, vol. 15, no. 1, pp. 403-462, 2024. [CrossRef] [Google Scholar] [Publisher Link]

[2] Muhammad Abdul Basit et al., “Limitations, Challenges, and Solution Approaches in Grid-Connected Renewable Energy Systems,” *International Journal of Energy Research*, vol. 44, no. 6, pp. 4132-4162, 2020. [CrossRef] [Google Scholar] [Publisher Link]

[3] Armin Razmjoo et al., “Stand-Alone Hybrid Energy Systems for Remote Area Power Generation,” *Energy Reports*, vol. 5, pp. 231-241, 2019. [CrossRef] [Google Scholar] [Publisher Link]

[4] Bhimsen Tudu et al., “Stand-Alone Hybrid Renewable Energy System-An Alternative to Increased Energy Demand,” *Proceedings of the 2014 International Conference on Control, Instrumentation, Energy and Communication (CIEC)*, Calcutta, India, pp. 335-339, 2014. [CrossRef] [Google Scholar] [Publisher Link]

[5] Subho Upadhyay, and M.P. Sharma, “Selection of a Suitable Energy Management Strategy for a Hybrid Energy System in a Remote Rural Area of India,” *Energy*, vol. 94, pp. 352-366, 2016. [CrossRef] [Google Scholar] [Publisher Link]

[6] Miloud Rezkallah et al., “Design and Implementation of Active Power Control with Improved P&O Method for Wind-PV-Battery-based Standalone Generation System,” *IEEE Transactions on Industrial Electronics*, vol. 65, no. 7, pp. 5590-5600, 2018. [CrossRef] [Google Scholar] [Publisher Link]

[7] Waqas Ali et al., "Design Considerations of Stand-Alone Solar Photovoltaic Systems," *2018 International Conference on Computing, Electronic and Electrical Engineering (ICE Cube)*, Quetta, Pakistan, pp. 1-6, 2018. [CrossRef] [Google Scholar] [Publisher Link]

[8] Shailendra Sharma, and Bhim Singh, "Permanent Magnet Brushless DC Generator based Stand-Alone Wind Energy Conversion System," *2013 4th IEEE International Symposium on Power Electronics for Distributed Generation Systems (PEDG)*, Rogers, AR, USA, pp. 1-6, 2013. [CrossRef] [Google Scholar] [Publisher Link]

[9] Ramadoni Syahputra, Kunnu Purwanto, and Indah Soesanti, "Performance Investigation of Standalone Wind Power System Equipped with Sinusoidal PWM Power Inverter for Household Consumer in Rural Areas of Indonesia," *Energy Reports*, vol. 8, pp. 4553-4569, 2022. [CrossRef] [Google Scholar] [Publisher Link]

[10] Dileep Kumar Varma Sagiraju, Yeddula Peda Obulesu, and Sai Babu Choppavarapu, "Dynamic Performance Improvement of Standalone Battery Integrated PMSG Wind Energy System using Proportional Resonant Controller," *Engineering Science and Technology, an International Journal*, vol. 20, no. 4, pp. 1353-1365, 2017. [CrossRef] [Google Scholar] [Publisher Link]

[11] M.R. Mostafa, Naggar Hassan Saad, and Ahmed Abd El-Sattar, "Tracking the Maximum Power Point of PV Array by Sliding Mode Control Method," *Ain Shams Engineering Journal*, vol. 11, no. 1, pp. 119-131, 2020. [CrossRef] [Google Scholar] [Publisher Link]

[12] Arslan Hameed et al., "Robust Sliding Mode Control based Maximum Power Point Tracking of Solar Photovoltaic System," *2020 3rd International Conference on Computing, Mathematics and Engineering Technologies (iCoMET)*, Sukkur, Pakistan, pp. 1-6, 2020. [CrossRef] [Google Scholar] [Publisher Link]

[13] Ghania Boudechiche et al., "Intelligent Solar Shunt Active Power Filter based on Direct Power Control Strategy," *Artificial Intelligence and Renewables Towards an Energy Transition*, Tipaza, Algeria, vol. 174, pp. 467-477, 2020. [CrossRef] [Google Scholar] [Publisher Link]

[14] B.G. Kavyashree, Shantharam Patil, and Vidya S. Rao, "Observer-based Anti-Windup Robust PID Controller for Performance Enhancement of Damped Outrigger Structure," *Innovative Infrastructure Solutions*, vol. 7, no. 3, pp. 1-16, 2022. [CrossRef] [Google Scholar] [Publisher Link]

[15] Rakesh Thankakan, and Edward Rajan Samuel Nadar, "Application of Fuzzy Logic-based MPPT Technique for Harvesting the Heat Energy Dissipated by the Wind Generator Stator Windings to Power Single-Phase Ac Grid Systems," *Neural Computing and Applications*, vol. 32, no. 18, pp. 15155-15170, 2020. [CrossRef] [Google Scholar] [Publisher Link]

[16] Rahul Kumar Rai, and O.P. Rahi, "Fuzzy Logic based Control Technique using MPPT for Solar PV System," *2022 First International Conference on Electrical, Electronics, Information and Communication Technologies (ICEEICT)*, Trichy, India, pp. 1-5, 2022. [CrossRef] [Google Scholar] [Publisher Link]

[17] Humam Al-Baidhani, and Marian K. Kazimierczuk, "Simplified Double-Integral Sliding-Mode Control of PWM DC-AC Converter with Constant Switching Frequency," *Applied Science*, vol. 12, no. 20, pp. 1-13, 2022. [CrossRef] [Google Scholar] [Publisher Link]

[18] Ricardo Lúcio de Araujo Ribeiro et al., "A Robust DC-Link Voltage Control Strategy to Enhance the Performance of Shunt Active Power Filters without Harmonic Detection Schemes," *IEEE Transactions on Industrial Electronics*, vol. 62, no. 2, pp. 803-813, 2015. [CrossRef] [Google Scholar] [Publisher Link]